SUPPLEMENTARY INFORMATION

Caves demonstrate decrease in rainfall recharge of southwest Australian groundwater is unprecedented for the last 800 years

Stacey C. Priestley[1,2,6]*, Pauline C. Treble[1,3], Alan D. Griffiths[1], Andy Baker[3], Nerilie J. Abram[4,5], Karina T. Meredith[1,3]

[1] ANSTO, Lucas Heights, NSW, Australia

[2] School of Physics, Chemistry and Earth Sciences, The University of Adelaide, Adelaide, SA, Australia

[3] School of Biological, Earth and Environmental Sciences, UNSW Sydney, Sydney, NSW, Australia

[4] Research School of Earth Sciences, Australian National University, Canberra, ACT, Australia

[5] ARC Centre of Excellence for Climate Extremes, Australian National University, Canberra, ACT, Australia

[6] Present address: CSIRO Environment, Glen Osmond, SA, Australia

*Corresponding author E-mail address: stacey.priestley@csiro.au

The Supplementary Information comprises:

Supplementary Note 1

Site description

Cave locations

All caves are located in the Leeuwin-Naturaliste National Park. All caves are developed in the Late Quaternary aeolian calcarenite[1,2] that outcrops along the coast of southwest Western Australia and receive rainfall from fronts embedded in the Southern Hemisphere mid-latitude westerly winds which are located over the region during the cooler months whilst rain events in summer are rare when the frontal systems pass further to the south. We provide a detailed description of the Golgotha Cave site below, being the most intensively studied cave and the location of the 14 years of dripwater monitoring presented in Figure 2 (main text). Table 1 (main text) summarises meta-data on each site including cave data, climate statistics and sources of previously published data. Stalagmite images photographed from slabs are shown in Supplementary Figure 1.

Golgotha Cave vegetation and soil

A mature wet eucalypt forest with 20-40 m tall canopy of karri and marri (*Eucalyptus diversicolor and Corymbia calophylla, syn. Eucalyptus calophylla*) and thick understorey overlies Golgotha Cave. Other caves studied are similarly located in *Eucalyptus* forest with dense understorey.

Golgotha Cave is covered in quartz-rich fine to coarse sand-sized particles with a high permeability that aids infiltration and reduces the potential for surface run-off. Infiltration is also aided by the fact that rain falls in the cooler months. Our soil moisture data[3,4] shows that soils become completely dry during the warmer months, due to high evapotranspiration rates. Thus when the next rainfall season begins, there is likely to be little to no contribution of isotopically-modified soil water and any contribution would be greatly diluted by the newly infiltrated water. Evapotranspiration occurs at these sites[5,6] (Table 1, main text) and this will also affect the volume of recharge as discussed in the main text.

Golgotha Cave host rock geology and flow paths

Golgotha Cave is formed in the Spearwood System of the coastal aeolinite that formed during the Late Quaternary[7]. Samples of the aeolinite host rock taken from the cave ceiling and the nearby cliff face were shown to contain porosities of 0.1-0.4[4]. The high porosity permits water movement through, and storage in, the aeolinite. Solution pipes with diameters ranging from 0.1 to >1 m are common and may act as vertical pathways with extremely high hydrological conductivity able to direct flow deep into the karst (Figure 2 in Ref. [4]). These may be closed at the base providing a store of water and promoting a stalactite cluster[8]. Preferential flow may also occur along fractures or interconnected fracture zones and bedding planes which, as described for the conduits, may not necessarily extend to the ceiling but promote preferential flow to depth. Images of such features taken in the field in the Spearwood System are shown in Supplementary Figure 3.

Electrical resistivity tomography in time-lapse mode (TL-ERT) was undertaken to image water movement from the soil to the cave ceiling between May 2016 and January 2018[4]. The spatial resolution of this technique is insufficient to resolve individual flow paths. However, it revealed zones of slow vertical percolation, interpreted to be diffuse flow predominately through the matrix, as well as faster moving vertical flow interpreted to be preferential recharge aided by the existence of higher permeability features such as conduits and fracture networks[4]. Water movement along these preferential recharge zones reached the ceiling to approximately 40 m depth in less than a year. While the TL-ERT study was unable to image individual flow paths, the existence of deep recharge along preferential flow paths is supported by drip rate monitoring and dripwater isotope observations in Golgotha Cave. In the longitudinal drip monitoring at Golgotha Cave in ref. [9] the drip rate for the site of stalagmite GL-S4 experienced a 6-fold threshold rise that was accompanied by a 0.5‰ drop in drip $\delta^{18}O$ in response to the 2013 rainfall season that experienced an annual total above the 90th percentile. The sudden rise in drip rate is characteristic of the relatively rapid and deep delivery of rainwater along a fracture[10]. Importantly this confirms the importance of seasonal saturation of the soil and epikarst zone to initiate recharge of karst stores above the monitored drip sites[4].

Hydrographs from 34 automatic drip loggers deployed in Golgotha Cave since 2012 show each drip site varies in characteristics such as base flow, rate of response to recharge, maximum drip rate and recession rate[11]. These drip data were compared with flow type classifications based on stalactite dimensions and spatial relationships on the ceiling[8,11] and confirmed that matrix flow dominated drips have low drip rates with low variability and includes smaller fractures; whereas drips associated with fractures exhibit a threshold rise in drip rate in response to preferential infiltration along a flow path that is otherwise supplied by water from the matrix[11]. Ref. [8] further described a flow type termed 'combination flow', describing flow through a larger network of fractures and conduits and where the conduit may be closed resulting in preferential flow to a circular feature of stalactites. It is thought that all drips in Golgotha Cave share the common hydrological domain of flow through the matrix, indicated by baseflow during reduced infiltration years, but with varying contribution of preferential flow as a function of infiltration and presence of fractures and other solutionally-widened features from the contributing flow paths[11,12]. Ref. [9] also presented dripwater $\delta^{18}O$ data from the flow path classified drip logger array and demonstrated an isotopic distinction between drips that are dominated by flow from the matrix (-4.0 ± 0.1‰, 1σ; n = 58) versus versus those more fracture and conduit flow influence (-4.7 ± 0.1‰, n = 22). These values should not be interpreted to represent the values of 'pure endmember' flow types, which in practice may not exist or have the properties required to develop a stalactite e.g., sufficient saturation with respect to calcite if a preferential flow path is involved. Rather, these values, and we infer all values of the studied dripwaters or those that fed the studied stalagmites represent mixtures of these flow types. A reduction in the processes that result in preferential flow (see main text) would result in an isotopic trend towards a higher value approaching values of dripwater predominately supplied by the matrix as is seen in the comparison of the composite uptick data and the distribution of the dripwaters in Figures 7a and 7b in the main text.

SUPPLEMENTARY TABLE 1: Campaign drip water data recorded for Golgotha Cave.

Site ID	Date collected (YYMMDD)	Duration of collection (days)	Flow type[1]	Drip rate (drips per minute)	$\delta^{18}O$ (‰$_{VSMOW}$)	δD (‰$_{VSMOW}$)
SW_1A	121024	2	Icicle	0.20	-4.2	-15.8
SW_1B	121024	2	Icicle	0.17	-4.2	-14.9
SW_1I	121024	2	Icicle	0.10	-3.8	-17.5
SW_1III	121024	2	Icicle	0.13	-3.5	-12.8
SW_1IV	121024	2	Icicle	0.30	-4.0	-15.8
SW_1VI	121024	2	Icicle	0.13	-3.5	-11.5
SW_1IX	121024	2	Icicle	0.17	-4.2	-17.9
SW_1XI	121024	2	Icicle	0.13	-4.3	-18.5
SW_2B	121024	2	Icicle	0.13	-3.9	-14.7
SW_2IV	121024	2	Icicle	0.03	-4.5	-20.2
SW_2VII	121024	2	Icicle	0.33	-3.7	-14.9
SW_2X	121024	2	Icicle	0.07	-3.7	-13.0
SW_1I	130604	2	Icicle	0.10	-3.4	-10.8
SW_1IV	130604	2	Icicle	0.28	-4.2	-13.9
SW_1VI	130604	2	Icicle	0.10	-3.3	-11.4
SW_1IX	130604	2	Icicle	0.18	-4.0	-15.3
SW_1XI	130604	2	Icicle	0.18	-4.3	-15.7
SW_2IV	130604	2	Icicle	0.17	-4.3	-17.1
SW_2VII	130604	2	Icicle	0.27	-4.2	-12.4
SW_2XIII	130604	2	Icicle	0.30	-4.4	-15.9
SW_2XIV	130604	2	Icicle	0.53	-5.1	-22.4
SW_2XV	130604	2	Icicle	0.17	-4.2	-15.8
SW_2XVII	130604	2	Icicle	0.07	-3.8	-13.1
SW_1A	130924	4	Icicle	0.23	-3.7	
SW_1B	130924	4	Icicle	0.16	-3.8	-15.6
SW_1I	130924	4	Icicle	0.08	-3.8	-12.1
SW_1III	130924	4	Icicle	0.09	-3.9	
SW_1IV	130924	4	Icicle	0.02	-4.0	
SW_1VI	130924	4	Icicle	0.10	-3.5	-10.7
SW_1IX	130924	4	Icicle	0.18	-3.9	-16.2
SW_1XI	130924	4	Icicle	0.16	-4.8	-17.7
SW_2A	130924	4	Icicle	0.12	-3.7	-11.7
SW_2B	130924	4	Icicle	0.21	-3.4	-8.9
SW_2IV	130924	4	Icicle	0.18	-4.1	
SW_2VII	130924	4	Icicle	0.29	-4.0	-14.3
SW_2X	130924	4	Icicle	0.07	-3.7	
SW_2XIII	130924	4	Icicle	0.33	-4.3	-15.0
SW_2XIV	130924	4	Icicle	0.28	-3.4	

SW_2XV	130924	4	Icicle	0.13	-4.2	
SW_SXVII	130924	4	Icicle	0.06	-3.1	-12.7
SW_1B	140220	5	Icicle	0.18	-4.1	-15.0
SW_1I	140220	5	Icicle	0.11	-3.8	-12.0
SW_1II	140220	5	Icicle	0.18	-4.1	-15.4
SW_1XI	140220	5	Icicle	0.23	-3.9	-14.7
SW_2A	140220	5	Icicle	0.08	-3.8	-14.5
SW_2B	140220	5	Icicle	0.21	-4.2	-13.9
SW_2IV	140220	5	Icicle	0.18	-4.2	-10.2
SW_2VII	140220	5	Icicle	0.40	-3.9	
SW_2X	140220	5	Icicle	0.11	-3.8	
SW_2XIV	140220	5	Icicle	0.56	-4.8	-19.0
SW_2XV	140220	5	Icicle	0.15	-4.4	-16.6
SW_2XVII	140220	5	Icicle	0.08	-3.6	-11.9
SW_2III	121024	2	Soda straw	0.07	-4.5	-18.0
SW_2III	130604	2	Soda straw	0.03	-4.4	-17.1
SW_1V	130924	4	Soda straw	0.07	-4.0	-13.8
SW_2III	130924	4	Soda straw	0.05	-4.2	-18.4
SW_1V	140220	5	Soda straw	0.13	-4.0	-13.2
SW_2III	140220	5	Soda straw	0.06	-4.9	
SW_1A	140609	5	Icicle	0.30	-4.2	-17.44
SW_1B	140609	5	Icicle	0.18	-4.4	-15.98
SW_1I	140609	5	Icicle	0.07	-3.9	-13.74
SW_1II	140609	5	Icicle	0.18		
SW_1III	140609	5	Icicle	0.12	-3.8	-12.37
SW_1IV	140609	5	Icicle	0.51	-4.1	-15.10
SW_1IX	140609	5	Icicle	0.22	-4.5	-17.83
SW_1VI	140609	5	Icicle	0.00	-3.8	-12.21
SW_1XI	140609	5	Icicle	0.24	-4.6	-18.65
SW_1XII	140609	5	Icicle	0.02	-3.8	-13.10
SW_2A	140609	5	Icicle	0.09		
SW_2B	140609	5	Icicle	0.22	-4.1	-14.96
SW_2IV	140609	5	Icicle	0.21	-4.7	-19.30
SW_2VII	140609	5	Icicle	0.35	-4.2	-14.98
SW_2X	140609	5	Icicle	0.11	-4.0	-14.56
SW_2XIII	140609	5	Icicle	0.33	-4.4	-17.63
SW_2XIV	140609	5	Icicle	0.60	-4.4	-17.93
SW_2XV	140609	5	Icicle	0.17	-4.2	-16.47
SW_2XVII	140609	5	Icicle	0.09	-3.8	-12.85
SW_1V	140609	5	Soda straw	0.13	-4.1	-15.58
SW_2III	140609	5	Soda straw	0.06	-4.5	-18.02
SW_2I	121024	2	Soda straw	3.33	-4.7	-22.1

SW_2VI	121024	2	Fracture	0.27	-3.9	-17.6
SW_2IX	121024	2	Fracture	4.67	-4.6	-19.1
SW_2II	121024	2	Fracture	1.00	-4.7	-21.0
SW_1X	130604	2	Fracture	0.80	-4.5	-19.1
SW_2I	130604	2	Fracture	3.13	-4.5	-21.1
SW_2VI	130604	2	Fracture	0.10	-4.8	-19.3
SW_2IX	130604	2	Fracture	4.67	-5.4	-19.8
SW_2XVI	130604	2	Fracture	1.67	-4.7	-19.1
SW_2II	130604	2	Fracture	2.47	-4.9	-22.6
SW_1X	130924	4	Fracture	0.96	-4.5	
SW_2I	130924	4	Fracture	3.10	-5.1	-22.3
SW_2VI	130924	4	Fracture	0.33	-4.9	-20.0
SW_2IX	130924	4	Fracture	4.50	-4.7	-20.4
SW_2XVI	130924	4	Fracture	1.33	-4.4	
SW_2II	130924	4	Fracture	3.03	-4.8	
SW_1X	140220	5	Fracture	1.42	-4.6	-19.5
SW_2I	140220	5	Fracture	3.20	-4.7	-17.9
SW_2VI	140220	5	Fracture	31.75	-4.5	
SW_2IX	140220	5	Fracture	4.77	-4.8	-19.9
SW_2XVI	140220	5	Fracture	6.08	-4.6	
SW_2II	140220	5	Fracture	2.00	-4.6	-19.8
SW_1VII	121024	2	Combined	0.93	-4.1	-12.3
SW_1VIII	121024	2	Combined	1.00	-4.1	-13.3
SW_2E	121024	2	Combined	2.00	-4.9	-22.5
SW_2V	121024	2	Combined	0.87	-3.8	-15.9
SW_2VIII	121024	2	Combined	1.67	-4.3	-17.1
SW_1VIII	130604	2	Combined	0.67	-3.7	-10.5
SW_2E	130604	2	Combined	1.82	-4.6	-19.7
SW_2V	130604	2	Combined	0.83	-4.4	-16.4
SW_2VIII	130604	2	Combined	1.13	-3.6	-12.3
SW_1VII	130924	4	Combined	1.14	-4.3	-13.1
SW_1VIII	130924	4	Combined	0.32	-3.5	-11.3
SW_2E	130924	4	Combined	1.80	-4.8	
SW_2V	130924	4	Combined	0.83	-4.4	-16.9
SW_2VIII	130924	4	Combined	1.26	-3.5	-11.0
SW_1VII	140220	5	Combined	0.38	-3.8	-11.9
SW_2E	140220	5	Combined	2.01	-4.9	-23.3
SW_2V	140220	5	Combined	0.95	-4.5	-19.1
SW_1VII	140609	5	Combined	1.82	-4.0	-13.51
SW_1VIII	140609	5	Combined	0.40	-3.9	-13.47
SW_2E	140609	5	Combined	2.00	-4.8	-20.29
SW_2V	140609	5	Combined	0.93	-4.4	-17.20

SW_2VIII	140609	5	Combined	1.52	-4.3	-17.15
SW_1X	140609	5	Fracture	0.92	-4.7	-19.20
SW_2I	140609	5	Fracture	3.32	-4.8	-20.61
SW_2II	140609	5	Fracture	0.88	-4.6	-19.40
SW_2IX	140609	5	Fracture	5.10	-4.8	-19.67
SW_2VI	140609	5	Fracture	35.06	-5.1	-20.03
SW_2XVI	140609	5	Fracture	5.31	-4.7	-19.41

[1] From ref. [8] icicle is diffuse flow dominated; soda straw is diffuse flow dominated; fracture is preferential flow influenced; combined is fracture network plus diffuse flow (preferential flow influenced)

SUPPLEMENTARY TABLE 2: Temperature data recorded for Golgotha Cave. All measurements made at the same location (drip sites GL-S1 and GL-S4) and show no trend through time.

Interval	**Logging interval (hours)**	**Mean ± 1 standard deviation (°C)**	**Type**	**Accuracy (°C)**
2005 - 2006	4	15.1 ± 0.1	Hobo Tidbit	± 0.2
2009 - 2011	0.25	14.8 ± 0.1	EL-USB-1-PRO temperature logger	± 0.2
2016 - 2022	0.25	14.6 ± 0.1	Vaisala independent temperature probe	± 0.13

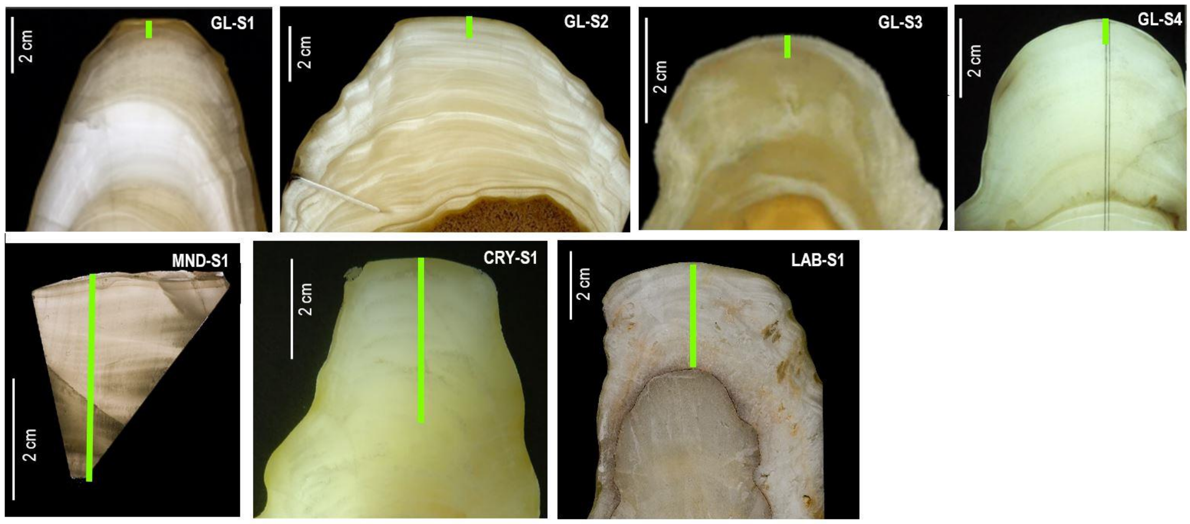

SUPPLEMENTARY FIGURE 1: Stalagmite images photographed from slabs approximately 5 mm thickness under transmitted or reflected light. Image for MND-S1 is a sub-section of cross-sectional slab. Green bar indicates growth sampled for $\delta^{18}O$ analyses presented in Figure 2 of main text. Stalagmites demonstrate variable widths indicative of changing drip rates that could indicate that drips were fed by a mixture of diffuse and preferential flow. All stalagmites are columnar and open-columnar fabrics (see for fabric descriptions ref. [13]).

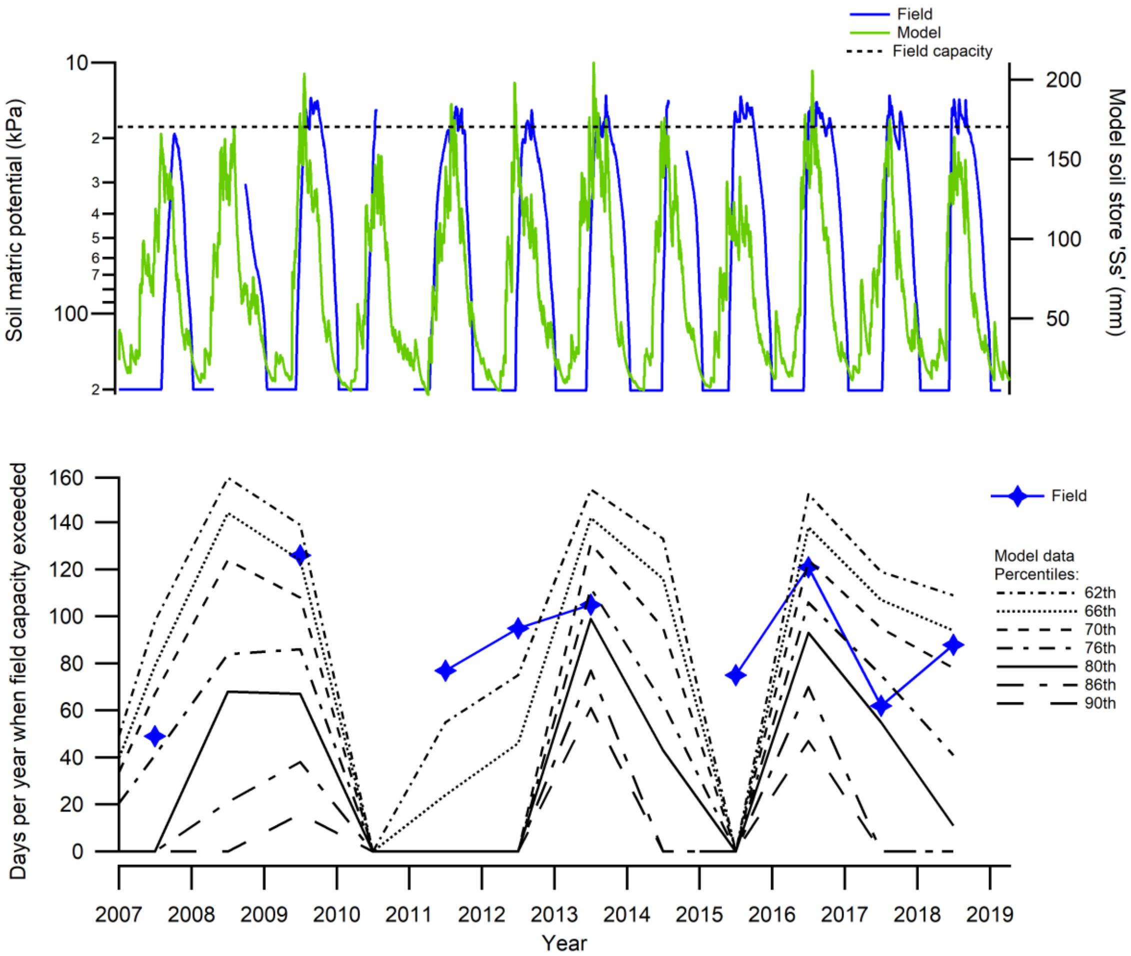

SUPPLEMENTARY FIGURE 2: Modelled versus field soil moisture observations for Golgotha Cave. Data in (a) are modelled soil moisture in the 0.1-1.0 m store layer (term Ss in AWRA-L model) compared with soil matric potential measured at 1.5 m depth at Golgotha Cave. The model results are representative of field conditions in terms of seasonality, the timing of seasonal wetting and the inter-annual variability in seasonal maxima and duration. Field soil matric potential data previously published in ref. [3] and updated to include data to 2018 here. Years 2013 and 2016 were two of the wettest years captured in our cave monitoring data and are confirmed to have initiated increased dripping from fracture flow paths recorded in our automatic drip logger network[4,11] and correspond with soil mean matric potential values of <18 kPa, in agreement with field capacity values for soils[14] with a high sand content. In Figure 3d (main text), we compare the number of days per year when modelled soil stores values represent saturated soils at each of the five cave sites. For these data, we used the AWRA-L model output from the deep soil store (1-6 m[15]; term Sd), as these depths corresponds with field observations of the depth of seasonal wetting prior to initiation of percolation to lower depths[4]. In order to compare model soil moisture values across the five cave sites we express Sd as the number of days per year when Sd is above a threshold percentile (b). Percentiles were calculated for the deep soil store for each cave site over the output period (1911-2018). The 66th percentile provided the least difference between the observed and modelled total number of days per year that field capacity was exceeded; however observed recharge at Golgotha during 2013 and 2016 suggests the 78th percentile would be representative of fracture activation necessary for recharge and we apply this to all 5 sites. The number of days above the 78th percentile was then calculated using Sd output for each cave site as shown in Figure 3 in the main text. All modelled data are from the Australian Bureau of Meteorology's Australian Water Resources Assessment Landscape model: AWRA-L version 6[16].

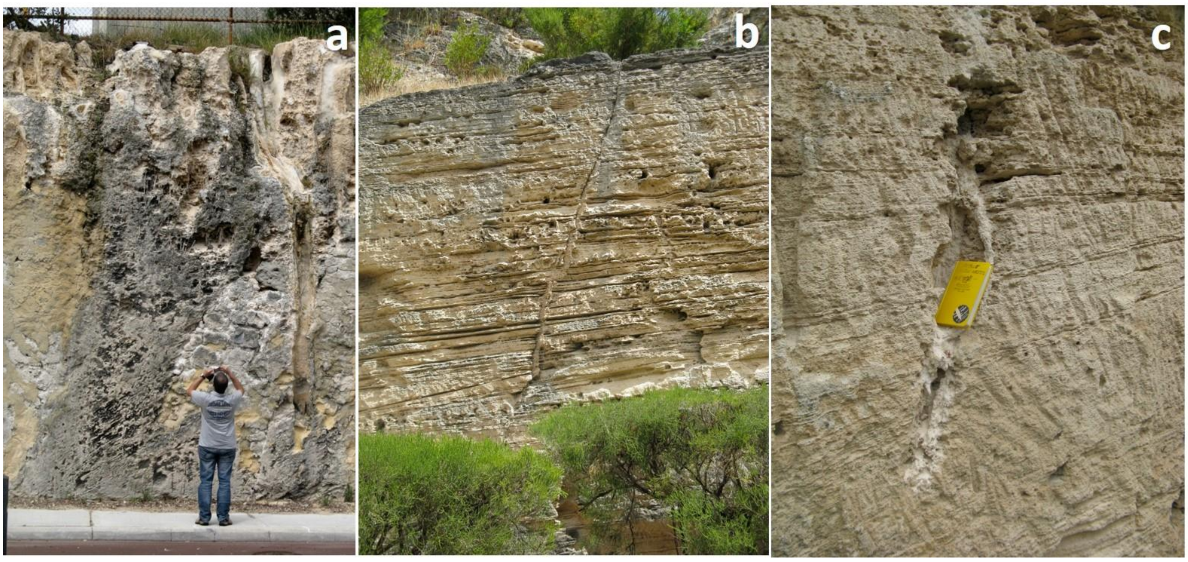

SUPPLEMENTARY FIGURE 3: Cross-sections of the Spearwood System in (a) road cutting in Fremantle, and (b,c) quarry in Floreat, (both Perth region) Western Australia. Vertical solution pipes and fractures are common and act as preferential flow paths supported by calcrete lining of these features. Person in (a) and large shrubs in (b) for scale indicate that these features can extend several meters or more.

SUPPLEMENTARY REFERENCES

1. Lipar M, Webb JA. Middle–late Pleistocene and Holocene chronostratigraphy and climate history of the Tamala Limestone, Cooloongup and Safety Bay Sands, Nambung National Park, southwestern Western Australia. *Aust J Earth Sci* 61(8)**,** 1023-1039 (2014).

2. Playford PE. *Geology of the Perth basin, Western Australia*. (Geological Survey of Western Australia: Perth, W.A., 1976).

3. Treble PC, Bradley C, Wood A, Baker A, Jex CN, Fairchild IJ*, et al.* An isotopic and modelling study of flow paths and storage in Quaternary calcarenite, SW Australia: implications for speleothem paleoclimate records. *Quat Sci Rev* 64**,** 90-103 (2013).

4. Leopold M, Gupanis-Broadway C, Baker A, Hankin S, Treble P. Time lapse electric resistivity tomography to portray infiltration and hydrologic flow paths from surface to cave. *J Hydrol* 593**,** 125810 (2021).

5. Treble PC, Fairchild IJ, Baker A, Meredith KT, Andersen MS, Salmon SU*, et al.* Roles of forest bioproductivity, transpiration and fire in a nine-year record of cave dripwater chemistry from southwest Australia. *Geochim Cosmochim Acta* 184**,** 132-150 (2016).

6. Nagra G, Treble PC, Andersen MS, Bajo P, Hellstrom J, Baker A. Dating stalagmites in mediterranean climates using annual trace element cycles. *Scientific Reports* 7(1)**,** 621 (2017).

7. Hall GJ, Marnham JR. *Regolith-landform Resources of the Karridale-tooker and Leeuwin 1:50000 Sheets*. (Dept. of Mineral and Petroleum Resources, Geological Survey of Western Australia: Perth, 2002).

8. Mahmud K, Mariethoz G, Treble PC, Baker A. Terrestrial LiDAR Survey and Morphological Analysis to Identify Infiltration Properties in the Tamala Limestone, Western Australia. *IEEE Journal of Selected Topics in Applied Earth Observations and Remote Sensing* 8(10)**,** 4871-4881 (2015).

9. Treble PC, Baker A, Abram NJ, Hellstrom JC, Crawford J, Gagan MK*, et al.* Ubiquitous karst hydrological control on speleothem oxygen isotope variability in a global study. *Communications Earth & Environment* 3(1)**,** 29 (2022).

10. Ireson AM, Butler AB, Wheater HS. Evidence for the onset and persistence with depth of preferential flow in unsaturated fractured porous media. *Hydrology Research* 43(5)**,** 707-719 (2012).

11. Mahmud K, Mariethoz G, Baker A, Treble PC, Markowska M, McGuire E. Estimation of deep infiltration in unsaturated limestone environments using cave lidar and drip count data. *Hydrol Earth Syst Sci* 20**,** 359–373 (2016).

12. Mahmud K, Mariethoz G, Baker A, Treble PC. Hydrological characterization of cave drip waters in a porous limestone: Golgotha Cave, Western Australia. *Hydrol Earth Syst Sci* 22(2)**,** 977-988 (2018).

13. Frisia S, Borsato A. Chapter 6 Karst. In: Alonso-Zarza AM, Tanner LH (eds). *Developments in Sedimentology*, vol. 61. (Elsevier, 2010).

14. Cassel DK, Nielsen DR. Field Capacity and Available Water Capacity. *Methods of Soil Analysis*, 1986).

15. Bureau of Meterology. Australian Landscape Water Balance. 2020 [cited 2020 November 2020] Available from: http://www.bom.gov.au/water/landscape/#/sm/Actual/day/-28.4/130.4/3/Point////2021/12/5/

16. Frost AJ, Ramchurn A, Smith A. The Australian Landscape Water Balance model (AWRA-L v6). Technical Description of the Australian Water Resources Assessment Landscape model version 6: Bureau of Meteorology Technical Report; 2018).